Compton polarimetry with a multi-layer CdTe focal plane prototype

M. Moita [a,b], E. Caroli [c], J.M. Maia [d,a], R.M. Curado da Silva [a,b,*], N. Auricchio [c], J.B. Stephen [c], M. Páscoa [a], A.M.F. Trindade [a,b]

[a] LIP-Laboratório de Instrumentação e Física Experimental de Partículas, Portugal
[b] Physics Department, University of Coimbra, Coimbra, Portugal
[c] INAF- Osservatorio di Astrofisica e Scienza dello spazio (OAS) di Bologna, Italy
[d] Physics Department, University of Beira-Interior, Covilhã, Portugal

ARTICLE INFO

Keywords:
Gamma-rays
X-rays
Polarimetry
CdTe
Astrophysics
Focal plane

ABSTRACT

In high-energy astrophysics, polarimetry is a promising subject with a wide scientific potential that is relatively unexplored due to the complexity of the design and technical requirements of the sensors. Often gamma-ray telescope proposals are based on multi-layer spectro-imager instruments with polarimetric capabilities. Herein we study a new Compton polarimeter prototype based on a two-layer CdTe pixelized spectro-imager operated in coincidence. The two CdTe detectors are 2 mm thick anode 8×8 pixels' segmented matrices with 2 mm pitch. This detection system configuration allows an assessment of the polarimetric potential of multi-layer solution focal planes as well as the polarimetric potential of a possible 3D spectro-imager by analysing the polarimetric performance when varying the distance between the two CdTe detection layers. The polarimetric modulation factors for single-layer (Q~0.4) and two-layer (up to 0.13) double-events were measured for 6 mm and for 10 mm distance between planes. The measured polarization angle resolution was lower than 10°. The potential of CdTe spectro-imager focal plane solutions with polarimetric capabilities for the next generation space missions based on both Laue lenses and 3D segmented focal planes is also discussed.

1. Introduction

Polarimetry in high-energy astrophysics has not been significantly explored due to the technical complexity of the required detection systems and analysis methods. Currently, no dedicated gamma-ray polarimeters are being operated successfully in space. In fact, X- and gamma-ray source emissions have been studied almost exclusively through 3 main observational parameters: spectral and timing analysis and by imaging techniques based on coded-mask cameras or telescopes equipped with high efficiency focal plane detectors. Polarization measurements will increase by two the number of observational parameters: (1) the polarization angle of the source emission; (2) the level of linear polarization of the same emission. These additional parameters should allow better discrimination between different emission models characterizing the same object. The polarimetric analysis of celestial sources can provide important information about the geometry, the magnetic field, the composition and the emission mechanisms. Polarized emissions are expected in a wide variety of gamma-ray sources such as pulsars, solar flares, active galactic nuclei, galactic black-holes and gamma-ray bursts [1–3]. In the soft gamma-ray domain (100 keV – 1 MeV), although some dedicated polarimeters have been proposed [4–11], only a few polarimetric measurements were performed by the INTEGRAL (INTErnational Gamma-Ray Astrophysics Laboratory) mission [12,13], on the Crab Pulsar, on the galactic black-hole Cygnus X-1 and on the gamma-ray burst GRB 041219A [14–17]. Presently, the importance high-energy polarimetry is finally widely recognized by the astrophysical community, especially with the new multi-messenger astrophysics, requiring that next generation of telescopes should provide fine polarimetric observation sensitivity together with increased energy, position and time resolution. Our team has been developing spectro-imager prototypes with polarimetric capabilities over more than a decade for high-energy space mission proposals submitted to ESA Cosmic Vision calls, such as: the GRI (Gamma-Ray Imager), DUAL and e-ASTROGAM [18–20]. These prototypes were semiconductor-based detection planes designed for coded mask and Laue lens instrument solutions for which an optimal trade-off between imaging, spectroscopy and polarimetry components was found.

A Laue Lens based gamma-ray telescope proposal, ASTENA (Advanced Surveyor of Transient Events and Nuclear Astrophysics), is being developed by the University of Ferrara, the INAF-OAS-Bologna and LIP [21]. The focal plane of this instrument will be composed either by segmented or 3D CdTe detectors. Within this scope, the aim of the experiment herein described is to study the potential performance of a Compton spectro-imager polarimeter in a two-layer configuration

based on CdTe pixelized detectors operated in coincidence. This experiment will contribute to the development of an optimized design of a CdTe Laue lens focal plane for polarimetric observations. The two-layer CdTe detectors are 2 mm thick, anode segmented matrices in an 8 × 8 pixels (2 mm pitch) format. This research work follows a series of successfully ESRF (European Synchrotron Radiation Facility) polarimetric experiments with a single matrix CdTe/CZT detectors in the 100–600 keV range, where measurement conditions were changed such as beam inclination, polarization level or direction as well as pixel size and thickness [22–27]. Since CdTe crystal growth with good characteristics is limited to less than ~10 mm thickness, multi-layer focal planes are a good solution to obtain high efficiency in the gamma-ray band. The new two-layer prototype configuration will allow an experimental assessment of the scattering polarimetric performance of a multi-layer instrument as well as the performance of a 3D spectro-imager, by simulating the effects on the performance when changing the distance between the two CdTe pixel detection layers. Previous work addressed these issues by analytical and simulation analysis [28,29]. The conclusions of this analysis will be a useful contribution for both high efficiency Laue lens telescope focal planes' and all sky advanced Compton telescopes' design for the next generation space missions, since both solutions would highly benefit from segmented 3D detection solutions to fulfil the requirements and optimize the telescope performance.

2. Compton polarimetry

The polarimetric performance of a high-energy detection plane is determined by the fundamental concepts associated with polarized Compton interactions and by its design. A polarized photon beam that is scattered by a detector element generates Compton scattered photons whose azimuthal distribution is modulated. Indeed, the scattered photons' angular direction depends on its initial polarization angle. If the scattered photon goes through a new interaction inside the detector, the statistical distribution of the photons' angular directions defined by the two interactions (double-event) provides a modulation curve whose degree and polarization direction of the incident beam can be derived. The azimuthal angular distribution of the scattered photons is given by the Klein–Nishina differential cross-section for linearly polarized photons:

$$\frac{d\sigma_{KN,P}}{d\Omega} = \frac{r_0^2}{2}\left(\frac{E'}{E}\right)^2\left[\frac{E'}{E} + \frac{E}{E'} - 2sin^2\theta\cos^2\phi\right], \quad (1)$$

where r_0 is the classical electron radius, E and E' are, respectively, the energies of the incoming and outgoing photons, θ the angle of the scattered photons and ϕ is the angle between the scattering plane (defined by the incoming and outgoing photon directions) and incident polarization plane (defined by the polarization direction and the direction of the incoming photon). As can be seen from (1), after fixing all other parameters the scattering probability varies with the azimuthal angle ϕ and its maximum and minimum arises for orthogonal directions. For ϕ=0° the cross-section reaches a minimum and for ϕ=90° the cross-section reaches a maximum.

The polarimetric performance of an instrument can be evaluated by calculating the polarimetric modulation factor, Q, of double-event distribution generated by a 100% polarized beam, and is defined as the amplitude of the modulation curve:

$$Q = \frac{N_{//} - N_{\perp}}{N_{//} + N_{\perp}}, \quad (2)$$

where $N_{//}$ *and* $N_{\perp}$, are the double-events integrated over two orthogonal directions defined over the detector plane along the maxima and minima of the modulation curve [30]. A higher value of Q means that a larger modulation is obtained in the double-events' distribution curve as a function of the azimuthal angle.

In the case of two-layer polarimeter (Fig. 1), we will assume the photons scattered in the top detector, depositing there part of their energy, and then absorbed by the bottom detector. The scattering direction is defined by the two pixels, one on the top and the other on the bottom layer, where the photon hits were recorded. In order to calculate the modulation factor, the events are selected in a hollow cone defined by θ_{min} and θ_{max} (Fig. 1). An estimate of the modulation factor as function of θ_{min} and θ_{max} can be computed taking into account the geometry of the instrument and the angular dependence of the differential cross section of Compton scattering. Using Eq. (2) the modulation factor is given by:

$$Q(\varepsilon, \theta_{min}, \theta_{max}) = \frac{M(\varepsilon, \phi = 90°, \theta_{min}, \theta_{max}) - M(\varepsilon, \phi = 0°, \theta_{min}, \theta_{max})}{M(\varepsilon, \phi = 90°, \theta_{min}, \theta_{max}) + M(\varepsilon, \phi = 0°, \theta_{min}, \theta_{max})}, \quad (3)$$

where ε is the energy of the incident photon in unit electron mass, of $\varepsilon = E / (m_e c^2)$ and M(ε, ϕ, θ_{min}, θ_{max}) is the modulation curve integrated over the range of θ values and can be derived using (1) and knowing the ratio between the photon energy before and after the scattering given

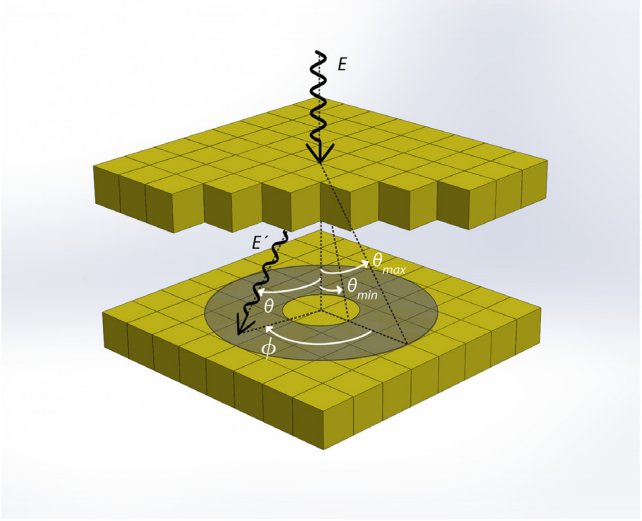

Fig. 1. Layout of a two-layer polarimeter. Polarization is measured by selecting the double-events scattered photons in the top detection plane and absorbed in the bottom detector. During each measurement, will be recorded the double-events scattered in the hollow cone defined by θ_{min} and θ_{max}.

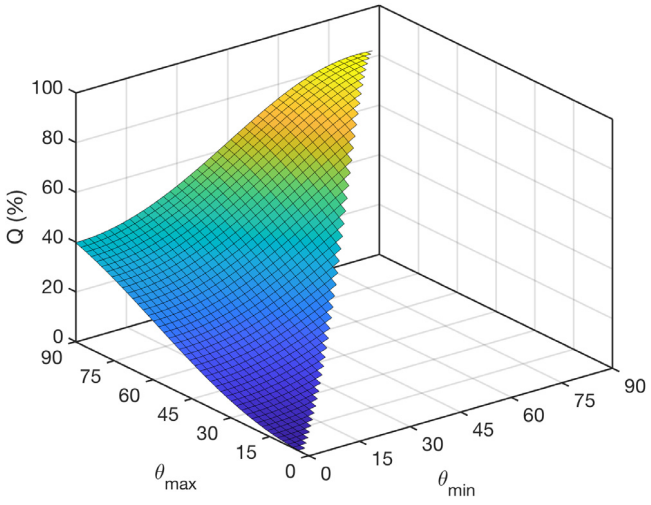

Fig. 2. Modulation factor as a function of maximum and minimum scattering angles θ_{min} and θ_{max} for a two-layer configuration, as in Fig. 1. The energy of the incident photons is 300 keV.

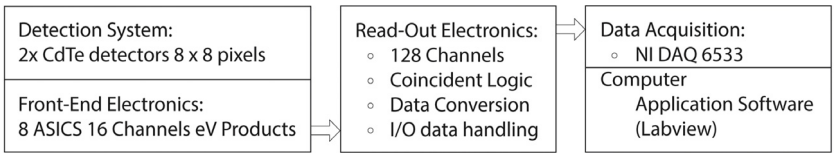

Fig. 3. Chain composing the prototype test system and the respective subsystems.

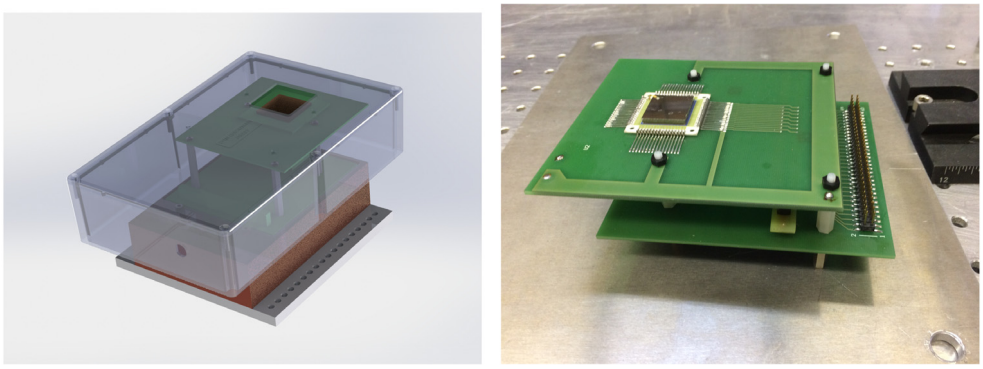

Fig. 4. (left) Schematic drawing of the POLCA IV detection system. The reddish box at the bottom is the POLCA FEE. The top enclosure is transparent to show the two detectors inside. (right) Picture the detection system. Each PCB shown support one of the detectors that are aligned in XY directions. The distance between the detectors can be adjusted.

by the Compton physics $E' = E\ /\ 1+\ \varepsilon\ (1-cos\theta)$:

$$M\left(\varepsilon,\varphi,\theta_{min},\theta_{max}\right) = \int_{\theta_{min}}^{\theta_{max}} \left(\frac{1}{1+\varepsilon(1-cos\theta)} + \frac{1}{[1+\varepsilon(1-\cos\theta)]^3} - \frac{2\sin^2\theta\cos^2\phi}{[1+\varepsilon(1-\cos\theta)]^2} \right) sin\theta\ d\theta, \quad (4)$$

In Fig. 2 we represent the modulation factor as a function of θ_{min} and θ_{max} for 300 keV photons. As can be seen the value of the modulation factor increases with θ_{min} and θ_{max} and the maximum modulation is obtained when θ_{min} and θ_{max} are about ~90°. This is the case of a thin single plane detector. In the case of our prototype, the values of θ_{min} and θ_{max} depend on the size of the detectors and the distance between them. Varying the distance between layers, we evaluated the modulation factor for different θ_{min} and θ_{max}. However, θ_{min} is limited by the low energy threshold of the top detector.

3. Experimental setup and methods

The two-layer polarimeter prototype was tested under a polarized beam generated at the ID (Insertion Device) 15A beamline of the ESRF [31]. The insertion device available was a U22 undulator, which provides a ~100% linearly polarized monochromatic photon beam from 30 up to 300 keV. However, during our test slots, the ID15A beamline energy was limited to a monochromatic beam of 278 keV. The beam flux after the monochromator in the optical hutch was of the order of 10^5 photons s^{-1} mm^{-2}. The prototype test system is composed by the following subsystems (Fig. 3): CdTe two-layer detection system; front-end electronics; read-out electronics; National Instruments data acquisition interface (NI DAQ); and application software.

The detection system is based on two ACRORAD CdTe detectors (product number P1P11616200P001 [32]), each detector with 2.0 mm thick. Each detection matrix was divided into 8 × 8 pixels with an area of 1.9 mm × 1.9 mm each, electrodes Pt/CdTe/Pt and 0.1 mm gap between consecutive pixels. The detectors were operated at room temperature with a bias voltage of 100 V. The average energy resolution of the matrix pixels was of about 7.5% @ 278 keV. In Fig. 4 is shown the CAD drawing of the POLCA IV system with the front-end electronics enclosure (red box) and the detector enclosure (transparent) with the two detectors inside. Also shown in Fig. 4 a picture of the two PCBs and the respective detectors.

The signals generated by the 128 pixels were read by the front-end electronics based on eight 16 channel eV-Products Application Specific Integrated Circuits (ASIC) [33]. Each channel consists of a charge sensitive amplifier followed by an active semi-Gaussian shaper (peaking-time of 1.2 μs). During the experiment the count rate was limited to 10^4 counts/s. The dead-time was ~1 μs. The signals were processed by a custom multiparametric system consisting of 128 independent channels with filters, coincidence logic and ADC (Analog-to-Digital Converter) units. The TAKES system allows the detector and pixel identification, and the energy measurement for each interaction in the detector pixels once the energy threshold for each interaction (~40 keV) and the time coincidence window (2 μs) are set. The coincidence logic is indispensable to select double-event detector hits and therefore to obtain the polarized beam modulation distribution in the matrix plane. When a pixel is hit by a photon releasing an energy above the low energy threshold, the system opens a coincidence window of 2 μs. For the pixels recording a signal above the threshold within this time interval, its position, energy and time tag are stored in a buffer (FIFO type). The data of each hit is coded in 32 bits and transferred to the output through a synchronized serial line at 10 MHz. The digital data was further processed and analysed by a PC-based data acquisition (DAQ) system, which is based on a National Instruments PCI-6533 board with 32 parallel digital inputs/outputs. The entire readout chain can handle up to ~10^4 counts/s. The DAQ was controlled by an algorithm written in LabView for Windows, allowing data management, storage on the PC's hard-disk and data quick look on the PC's screen.

The detector was mounted perpendicular to the beam inside a rotational stage on a XYZ positioning system as can be seen in Fig. 5. The detector subsystems (detector, power supply, multiparametric electronics) have been mounted inside the experimental hutch, leaving in the control room the serial to parallel interface box and the PC for data acquisition and screen quick-look. The ESRF control console allowed the management of the detector position and rotation as well as the hutch shutter and the absorber positioning.

There are several effects that under certain conditions might introduce significant errors in the modulation factor measurement. However, for CdTe pixelized matrices the dominant source of error is the non-uniformity in pixel response due to material imperfections throughout the matrix bloc. It may vary by more than 25% for a significant fraction of the pixels. Another important source of systematic errors is related to our experiment, in particular the alignment accuracy of the beam

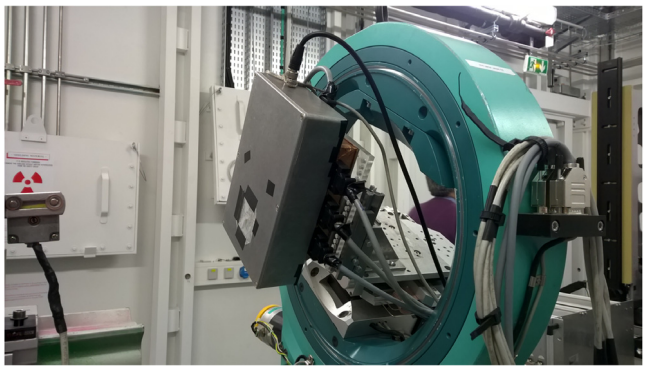

Fig. 5. The detection system case mounted on a mechanical ESRF ring that was remotely controlled for azimuthal rotation and XYZ micrometric positioning.

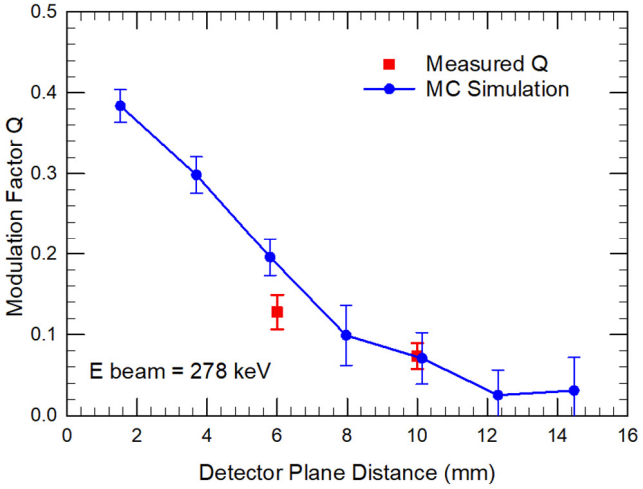

Fig. 6. The modulation factor Q measured for 278 keV photons at two different distances between the detector planes compared with the simulation curve for modulation obtained for the full target distance range of the Compton-POLCA system (2–16 mm).

with respect to the irradiated pixel centre and the alignment between detectors. In order to minimize these sources of error before each measurement we performed a complete scan of all detector pixels. This scan was performed with ESRF beam at 278 keV for both detectors at the laboratory with an uncollimated source. In order to compensate for any misalignment of the detectors, each pixel was divided in 16 sub-pixels that were scanned with a 0.5 × 0.5 mm^2 beam for 10 s each, carrying out 1024 steps in total. The matrix of each detector obtained from the single events recorded in each pixel was then used to correct the inherent non-uniformities in the response of the detector pixels. We estimate the true double-event counts for each pixel by:

$$N_{true} = \frac{N_{pol}}{N_{non}} N_{max}, \tag{5}$$

where N_{pol} is the number of double-events detected (that depend on the beam polarization), N_{non} is the number of single events of the response map obtained when the pixel is directly irradiated and N_{max} the is maximum value among all the matrix pixels single events. By applying this method to the pixels surrounding the irradiated pixel, the error introduced by the non-uniformity of the detector matrix response is minimized thereby improving the precision of the calculated modulation factor.

To evaluate the polarimetric performance we selected the double-events in each measurement. We divided them between single-layer (double-event in the same plane) events and two-layer (double-event interacting in the top and in the bottom layers) events. Multiple events do not enter into our calculations since we cannot determine the order of each hit. For double-events, we know the position of the first interaction, that corresponds to the position of the irradiated pixel by the collimated beam, therefore during the analysis we exclude double-events that do not have at least one interaction in the target pixel, e.g., chance coincidence events due to noise and flaring pixels and/or triple events in which the first interaction in the target pixel was under the low energy threshold. Because of the ESRF beam was monochromatic we also applied a simple selection of double-events using the energy deposited in each hit. Knowing the beam initial energy, we selected the double-events for which the total energy of the two interactions matches the beam energy within the limits of detectors' energy resolution. The spurious coincidences are largely removed due to the knowledge of the incoming beam energy and to the Compton kinematics analysis. In the case of the two-layer interactions, the energy of the events depends on the possible scattering angles, therefore the selection is performed within an energy range compatible with possible angles. Lastly, due to the low energy threshold of the system, ~40 keV, we expected that the minimum scattering angle is ~40°, therefore double-event angles below this angle were excluded. Very low efficiency backscattered events from the electronics under the second plane do not affect the measurements. These photons' energy range up to ~100 keV, where those below the threshold are eliminated and the remaining are absorbed as single events.

In order to optimize the double-event histogram readout, we applied the radial bin technique (RBT) [1], by dividing the matrix into 24 radial bins of 15° each. Pixels partially crossed by angular bin lines contribute only with a fraction of the number of events equal to the fraction of its area that is in the sector – this is an approximation since real hits inside each pixel are not uniformly distributed but have a radial dependence relative to the position of the first Compton interaction of a double-event. The modulation curve, $N(\varphi)$, giving the number of double-events as a function of the azimuthal angle φ, was then obtained. The polarimetric modulation factor Q was calculated from (3) and the polarization direction was obtained from the angle that maximizes (3). These data correction and analysis techniques were processed by a MatLab based code [34].

4. Experimental results analysis

4.1. Single layer polarimetric performance

Before performing two-layer polarimetric measurements, we analysed the specific polarimetric performance of each detection layer, in order to better interpret the results obtained when performing polarimetric measurements with the two detection layers.

Even though, ID15A beamline energy was limited to a 278 keV monochromatic beam, previous polarimetric studies with single plane CdTe based detectors with similar characteristics have shown that the best modulation Q factor is obtained in the energy range between 200 keV and 400 keV (for a Q factor between ~0.3 and ~0.4), since at these energies a larger fraction of photons is scattered at angles closer to 90° [22–27]. Typical efficiencies obtained were of about 70% for single events and 10% for double-events. Operating the setup shown in Fig. 5, a polarized beam was generated, irradiating one of the central pixels of the top layer for a count rate limited to 10^4 counts/s. The number of recorded double-events ranged from ~10^4 up to 10^5 per pixel. Afterwards, we repeated the same procedure but this time irradiating a central pixel of the bottom layer. The modulation factors obtained were 0.46 ± 0.01 and 0.37 ± 0.02 for the top and bottom layer respectively. The difference between the polarimetric modulation factors obtained in each of the two detection layers was essentially conditioned by the number of noisy and dead pixels of each layer. In the top layer we identified ~30 faulty pixels and ~15 in the bottom layer. Noisy pixels were fundamentally due to imperfections generated during the bonding

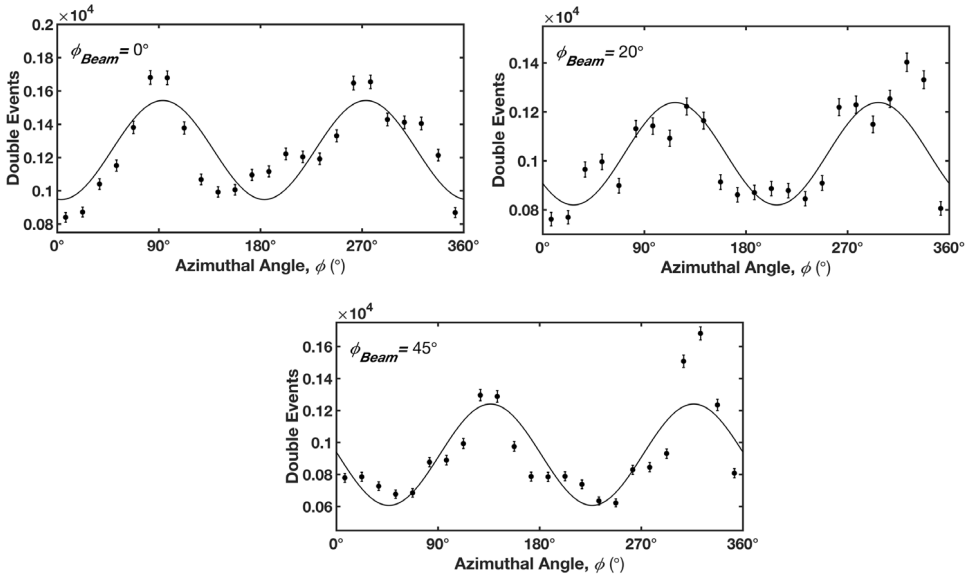

Fig. 7. Number of double-events obtained inside a 15° radial bin, centred on the CdTe pixelized matrix for polarization angles of: 0°, 20° and 45° (fitted sinusoid represented just for guideline purposes).

process performed by the company that provided this service. The measured residual modulation obtained in each layer when irradiating with a non-polarized beam was on average 0.05 ± 0.01.

4.2. Modulation factor vs. distance

The aim of this experiment was to evaluate the modulation factor Q for different distances between detectors. The methodology herein applied was performed by pointing the ID15A collimated beam onto the top detector and by selecting and analysing the double-events that interacted in the top plane and on the bottom plane. One of the 4 central pixels on the top layer was irradiated. The analysis considered the asymmetry of irradiating one of the 4 central pixels of an 8 × 8 matrix. Therefore, the double-event distribution spread from the corresponding bottom central pixel (aligned with the irradiated one) up to fourth order pixels, for two distances between detectors: 6 mm and 10 mm.

Observed experimental results presented in Fig. 6 show a decrease of the modulation factor when the distance between planes was increased, as expected, since as the scattering angle range decreases and the modulation also decreases noticeably, as illustrated in Fig. 2, representing the modulation a function of the scattering angles. Furthermore, in Fig. 6 it is also represented the simulation curve for modulation factor Q at 278 keV for the full target distance range of the Compton-POLCA system (2–16 mm). In this simulation code was modelized the main geometrical parameters of the system (lateral size, pixel pitch, distance between planes, etc.) as well as the measured response of the individual pixels of the top (only the irradiated pixel) and the bottom matrix was included in the code. The simulated double-event efficiency between planes was ~5%. Results show a good agreement of the trends of both experimental and simulated results, a with slight lower modulation level for the 6 mm measurements, that can be due to several other effects not included in the simulation code (eventual minor axial or rotational misalignment between the planes, individual pixel response change with time, etc.).

Interpreting the results represented in Fig. 6, we can conclude that the contribution for the instrument modulation of double-events recorded between different material layers depends significantly from the distance between the triggered layers. Then, the distance between layers is an essential parameter to consider when designing and dimension a multi-layer instrument or projecting a 3D detector for high-energy polarimetry. Other relevant factors that determine the polarization sensitivity were previously addressed in preceding experiments and simulations with similar CdTe prototypes such as the single, double and multiple detection efficiency, in and off-axis detection, modulation dependence on pixel size and thickness, modulation invariance to Laue diffraction and polarization sensitivity improvement with Laue lens focusing systems [22–27]. The advantages of operating Laue lens based instrument, such as improved source position resolution or signal-to-noise ratio, are discussed in detail together with a variety of factors affecting in-orbit polarization sensitivity in [35]. In order to build a credible realistic mission scenario all these factors must be considered and properly weighted with in-orbit background level as well as with background rejection techniques and event reconstruction methods (~40% event reconstruction level can be achieved in this energy range applying methods in [36]).

4.3. Polarization angle measurements

Subsequently, we analysed the dual-plane detector potential to determine the polarization angle orientation. These tests were done by positioning the collimated beam (1×1 mm^2 beamspot) onto a top plane central pixel, after rotating the detector, firstly by 20° and afterwards by 45°. The distance between planes was 6 mm. The modulation of the double-events distribution recorded inside a 15° radial bin centred on the CdTe pixel matrix was estimated by selecting the number of events in each pixel of the bottom detector. Fig. 7 illustrates the modulation (fitted sinusoid represented just for guideline purposes) obtained when the beam polarization is oriented through 0°, 20°, and 45°. As expected from theory, for a polarization angle of 0° a maximum number of Compton photons were detected in the perpendicular direction with respect to the polarization direction. Inside the experimental hutch it corresponds to the vertical direction. This matches with the fact that the beam polarization is horizontal inside the hutch since the polarization is always perpendicular to the maximum intensity direction.

The measured angles were 2.0° ± 8.5°, 25.0° ± 6.0° and 46.3° ± 3.2° for the effective ESRF beam polarization angle of 0°, 20 and 45°, respectively. Therefore, polarization angles can be determined with a resolution lower than 10°. Fig. 8 shows the measured polarization angle (φ_{obs}) as a function of the effective ESRF beam polarization angle (φ_{beam}) at 278 keV. The linear fit calculated is also represented. Overall analysis of these results shows a good agreement between measured polarization angle and the effective beam polarization angle, in accordance with the previous studies [26].

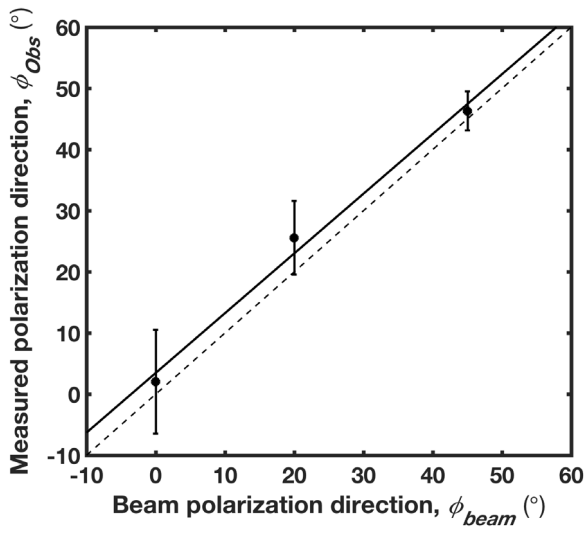

Fig. 8. The measured polarization angle as a function of the effective ESRF beam polarization angle for 278 keV. The errors associated to each measured polarization angle were obtained by averaging the angle of the two maxima and the two minima of each double-event modulation curve applying a 90° independent partial fitting, since the polarization is 90° symmetric. A linear fitting was applied: $\varphi_{obs} = 0.95\ \varphi_{beam} + 5.23$ and is represented by the solid line. The dotted line represents the expected result were $\varphi_{obs} = \varphi_{beam}$.

5. Conclusions

Herein, were presented the polarimetric performances of a two-layer CdTe prototype under a polarized gamma-ray beam, obtaining consistent results with the expected theoretical polarimetric potential of this kind of prototype configuration. The *Q* modulation factors were measured for the individual CdTe layers (~ 0.40). When operating the prototype in the two-layer Compton polarimetric mode, we observed that the *Q* factor decreased with the distance between layers as expected, since in this energy range the modulation is maximized for scattering angles ~ 90°, decreasing the modulation as the scattering angle decreases to shallow angles. Modulation Q factors of ~ 0.13 and ~ 0.08 were obtained respectively for 6 mm and for 10 mm distance between planes. When combined with single- and two-layer modes, high polarimetric performances can be achieved, with the advantage of the high detection efficiency provided by the multi-layer solution. Presenting a good intrinsic modulation factor as well as a high detection efficiency, this configuration provides optimal low minimum detectable polarization levels. Measurements also show that a polarization angular resolution lower than 10° can be achieved in the two-layer mode. These results confirm the fine polarimetric potential of multi-layer configuration CdTe focal planes, even when considering the main relevant factors affecting the polarimetric sensitivity of an instrument previously addressed by our groups (efficiency, pixel size and thickness, reconstruction, in and off-axis source emissions, etc.). Furthermore, this study paves the way for an experiment in preparation where the polarimetric performance of a small two-layer prototype as a function of two-layer distance will be performed with increased detail, (millimetric or submillimetric steps) so as to be able to reconstruct the complete response as a polarimeter of a realistic 3D detector. Highly segmented 3D detection systems together with the multi-layer configuration, are the focal plane configurations under study for the ASTENA Laue lens telescope proposal.

Acknowledgments

Miguel Moita was supported by a Doctorate in Applied and Engineering Physics fellowship (PD/BD/105922/2014), a FCT funded Ph.D. program. Alexandre Trindade was supported by FCT (Fundação para a Ciência e a Tecnologia) Ph.D. fellowship SFRH/BD/116825/2016. The ESRF supported the travel expenses of Jorge Maia, Marcela Páscoa, and Miguel Moita during the described experiment performed at the European Synchrotron.

References

[1] F. Lei, A.J. Dean, G.L. Hills, Compton polarimetry in gamma-ray astronomy, Space Sci. Rev. 82 (1997) 309–388.
[2] R. Bellazzini, et al., X-ray Polarimetry: A New Window in Astrophysics, eds. Cambridge University Press, 2010.
[3] Mark McConnell, et al., X-ray and Gamma-Ray Polarimetry, Astro2010: The Astronomy and Astrophysics Decadal Survey, Science White Papers, no. 198, 2009.
[4] E. Suarez-Garcia, W. Hajdas, POLAR: Design of a novel X-ray polarimeter based on plastic scintillators and MAPMTs, Nucl. Instrum. Methods A (610) (2009) 276–279.
[5] Y. Kishimoto, Basic performance of PHENEX: A polarimeter for high ENErgy X rays, IEEE Trans. Nucl. Sci. 54 (3) (2007) 561–566.
[6] H. Krawczynski, A. Garson III, J. Martin, et al., The Hard X-ray Polarization Sensitivity of the Energetic X-ray Imaging Survey Telescope EXIST, PoS(CRAB2008) 026.
[7] J.E. Hill, M.L. McConnell, P. Bloser, et al., POET: POlarimeters for energetic transients, in: AIP Conf. Proc., Vol. 1065, 2008, p. 331.
[8] J. Greiner, A. Iyudin, G. Kanbach, Gamma-ray burst investigation via polarimetry and spectroscopy (GRIPS), Exp. Astron. 23 (1) (2009) 91–120.
[9] H. Tajima, R. Blandford, T. Enoto, et al., Soft gamma-ray detector for the ASTRO-H mission, in: Proc. of the SPIE, Vol. 7732, 2010, pp. 773216–773216–17.
[10] D. Yonetoku, T. Murakami, S. Gunji, Gamma-Ray burst polarimeter - GAP - aboard the small solar power sail demonstrator IKAROS, Astron. Soc. Japan 63 (2011) 625.
[11] T. Kamae, et al., PoGOLite –A high sensitivity balloon-borne soft gamma-ray polarimeter, Astropart. Phys. 30 (2008) 72–84.
[12] C. Winkler, T.J. Courvosier, et al., The integral mission, Astron. Astrophys. 411 (2003) L1–L6.
[13] P. Ubertini, F. Lebrun, G. Di Cocco, et al., IBIS: The imager on-board INTEGRAL, Astron. Astrophys. 411 (2003) L131–L139.
[14] A.J. Dean, et al., Polarized gamma ray emission from the CRAB, Science 321 (5893) (2008) 1183–1185.
[15] M. Forot, et al., Polarization of the crab pulsar and nebula as observed by the INTEGRAL/IBIS telescope, Astrophys. J. 688 (2008) L29–L32.
[16] P. Laurent, J. Rodriguez, J. Wilms, et al., Polarized gamma-ray emission from the galactic black hole cygnus X-1, Science 332 (6028) (2011) 438–439.
[17] D. Götz, P. Laurent, F. Lebrun, et al., Variable polarization measured in the prompt emission of GRB 041219A using IBIS on board INTEGRAL, Astrophys. J. Lett. 695 (2009) 2.
[18] J. Knödlseder, et al., GRI: focusing on the evolving violent universe, in: S.L. O'Dell, G. Pareschi (Eds.), Proc. SPIE on Optics for EUV, X-Ray, and Gamma-Ray Astronomy III, Vol. 6688, 2007, p. 668806.
[19] P. von Ballmoos, T. Takahashi, S.E. Boggs, A DUAL mission for nuclear astrophysics, Nucl. Instrum. Methods A623 (2010) 431–433.
[20] De Angelis, et al., The e-ASTROGAM mission: Exploring the extreme Universe with gamma rays in the MeV - GeV range, Exp. Astron. 44 (1) (2017) 25–82.
[21] Virgilli Curado da Silva, et al., The Advanced Surveyor of Transient Events and Nuclear Astrophysics (ASTENA) mission within AHEAD project, SPIE Astron. Tel. Austin, USA, 2018.
[22] R.M. Curado da Silva, E. Caroli, N. Auricchio, et al., Hard-X and soft gamma-ray polarimetry with CdTe array prototypes, IEEE Trans. Nucl. Sci. 51 (5) (2004) 2478–2484.
[23] R.M. Curado da Silva, et al., Polarimetric performance of a Laue lens gamma-ray CdZnTe focal plane prototype, J. Appl. Phys. 104 (8) (2008) 084903.
[24] Ezio Caroli, Rui M. Curado da Silva, John B. Stephen, et al., A polarimetric experiment with a laue lens and CZT pixel detector, IEEE Trans. Nucl. Sci. 56 (4) (2009) 1848–1854.
[25] R.M. Curado da Silva, N. Auricchio, E. Caroli, et al., Polarimetry study with a CdZnTe focal plane detector, IEEE Trans. Nucl. Sci. 58 (4) (2011) 2118–2123.
[26] R.M. Curado da Silva, E. Caroli, J.B. Stephen, N. Auricchio, J.M. Maia, et al., Polarization degree and direction angle effects on a CdZnTe focal plane performance, IEEE Trans. Nucl. Sci. 59 (4) (2012) 1628–1635.
[27] S. Antier, P. Ferrando, O. Limousin, E. Caroli, R.M. Curado da Silva, et al., Hard X-ray polarimetry with Caliste, a high performance CdTe based imaging spectrometer, Exp. Astron. 39 (2) (2015) 233–258.
[28] F. Muleri, R. Campana, Sensitivity of stacked imaging detectors to hard X-ray polarization, Astrophys. J. 751 (2) (2012) 88–99.
[29] N. Auricchio, E. Caroli, A. Basili, et al., Development of a CZT spectroscopic 3D imager prototype for hard X ray astronomy, IEEE NSS and MIC, Oct. 27-Nov. 2, Seoul, South Korea, 2013.
[30] M. Suffert, P.M. Endt, A.M. Hoogenboom, Polarization measurements of proton capture gamma rays, Physica 25 (1959) 659.
[31] J. Chavanne, P. Elleaume, Rev. Sci. Instrum. 66 (2) (1995) 1868–1871.
[32] Retrieved from CdTe Acrorad Standar Products: https://www.acrorad.co.jp/index_en/products_en/cdte/cdte_products.html#5.
[33] G. De Geronimo, P. O'Connor, A. Kandasamy, Proc. SPIE 4784 (2003) 105.
[34] MATLAB version 7.10.0. Natick, Massachusetts: The MathWorks Inc., 2010.
[35] Curado da Silva, et al., Chapter 10: CdZnTe 2D/3D spectrometers for scattering polarimetry, in: Semiconductor Radiation Detectors: Technology and Applications, CRC Press, Boca Raton, 2017, pp. 241–282.
[36] Zoglauer, et al., MEGAlib–The medium energy gamma-ray astronomy library, New Astron. Rev. 50 (2006) 629.